Secondary formation of nitrated phenols: insights from observations during the Uintah Basin Winter Ozone Study (UBWOS) 2014

Bin Yuan[1,2], John Liggio[3], Jeremy Wentzell[3], Shao-Meng Li[3], Harald Stark[2,4], James M. Roberts[1], Jessica Gilman[1,2], Brian Lerner[1,2], Carsten Warneke[1,2], Rui Li[1,2], Amy Leithead[3], Hans D. Osthoff[5], Robert Wild[1,2], Steven S. Brown[1,6], and Joost A. de Gouw[1,2,6]

1. NOAA Earth System Research Laboratory (ESRL), Chemical Sciences Division, Boulder, CO, USA
2. Cooperative Institute for Research in Environmental Sciences, University of Colorado at Boulder, Boulder, CO, USA
3. Environment Canada, Science and Technology Branch, Toronto, ON, Canada
4. Aerodyne Research Inc., Billerica, MA, USA
5. Department of Chemistry, University of Calgary, Calgary, Canada
6. Department of Chemistry and Biochemistry, University of Colorado at Boulder, CO, USA

Abstract

We describe the results from online measurements of nitrated phenols using a time of flight chemical ionization mass spectrometer (ToF-CIMS) with acetate as reagent ion in an oil and gas production region in January and February of 2014. Strong diurnal profiles were observed for nitrated phenols, with concentration maxima at night. Based on known markers (CH_4, NO_x, CO_2), primary emissions of nitrated phenols were not important in this study. A box model was used to simulate secondary formation of phenol, nitrophenol (NP) and dinitrophenols (DNP). The box model results indicate that oxidation of aromatics in the gas phase can explain the observed concentrations of NP and DNP in this study. Photolysis was the most efficient loss pathway for NP in the gas phase. We show that aqueous-phase reactions and heterogeneous reactions were minor sources of nitrated phenols in our study. This study demonstrates that the emergence of new ToF-CIMS (including PTR-TOF) techniques allows for the measurement of intermediate oxygenates at low levels and these measurements improve our understanding of the evolution of primary VOCs in the atmosphere.

1. Introduction

Nitrated phenols are a family of aromatic compounds with both nitro (-NO_2) and hydroxyl groups (-OH) connected to a benzene ring. Nitrated phenols have been detected in the gas phase, aerosol, cloud water and rainwater (Harrison et al., 2005a). Many studies have shown that nitrated phenols are one of the important components of brown carbon in aerosol (Desyaterik et al., 2013;Mohr et al., 2013;Zhang et al., 2013;Lin et al., 2015), as they absorb light in the atmosphere (Bejan et al., 2007). Photolysis of some nitrated phenols was reported to produce nitrous acid (HONO) (Bejan et al., 2006) and hydroxyl (OH) radicals (Cheng et al., 2009), while the oxidation and photolysis of them contribute to secondary organic aerosol (SOA) formation, especially in biomass burning plumes (Mohr et al., 2013;Kitanovski et al., 2012;Lauraguais et al., 2014). There is also evidence that nitrated phenols are phytotoxic and contribute to forest decline (Rippen et al., 1987;Natangelo et al., 1999). Some nitrated phenols are known to be mutagenic and are of concern to human health (Fernandez et al., 1992).

Sources of nitrated phenols in the atmosphere include emissions from vehicle exhaust (Inomata et al., 2013;Tremp et al., 1993;Sekimoto et al., 2013) and biomass burning (Mohr et al., 2013). Nitrated phenols are also produced from photooxidation of aromatic hydrocarbons in the atmosphere: for example benzene oxidizes to 2-nitrophenol (2-NP) and 4-nitrophenol (4-NP), and toluene oxidizes to methylnitrophenols (MNP) (Harrison et al., 2005a). Figure 1 shows the reactions leading to secondary formation of NP and dinitrophenols (DNP) in the atmosphere (Jenkin et al., 2003). Oxidation of benzene by OH radicals forms phenol and further reactions of phenol with either OH or NO_3 radicals yield phenoxy (C_6H_5O) radicals, which react further with NO_2 to generate NP. In addition to benzene oxidation, C_6H_5O radical is also generated from the reaction of NO with phenyl peroxy ($C_6H_5O_2$) radicals, a product from reactions of some other aromatic precursors, e.g. benzaldehyde (Caralp et al., 1999). Further oxidation of nitrated phenols by obtaining another nitro- group produces dinitrophenols (DNP). The yields of NP from phenol oxidation by OH radicals (Atkinson et al., 1992;Olariu et al., 2002;Berndt and Boge, 2003) and NO_3 radicals (Atkinson et al., 1992;Bolzacchini et al., 2001) have been reported. Berndt and Boge (2003) also showed that the NP yield from

OH oxidation of phenol increases at higher NO_2 concentrations. In addition to gas phase reactions, nitrated phenols are formed from aqueous-phase reactions in aerosol or cloud water (Vione et al., 2001, 2005). The importance of the aqueous reactions compared to gas-phase reactions is highly dependent on liquid water content in the atmosphere (Harrison et al., 2005b).

The sinks of nitrated phenols in the gas phase include reactions with OH radicals (Atkinson et al., 1992;Bejan et al., 2007), with NO_3 radicals (Atkinson et al., 1992), with chlorine atoms (Bejan et al., 2015) and photolysis (Bejan et al., 2007;Chen et al., 2011). It has been proposed that photolysis is the dominant gas phase atmospheric loss for nitrated phenols (Bejan et al., 2007). Despite the importance of photolysis of nitrated phenols, the photolysis frequency of nitrated phenols under ambient conditions was only reported in a single non-peer reviewed publication (1.4% of photolysis frequency of NO_2) (Bardini, 2006). The chemical products from photolysis of nitrated phenols were proposed, but the proposed products were not fully evaluated against experimental results (Bejan et al., 2006). Nitrated phenols are also removed by various processes in the aqueous phase, including reactions with OH, NO_3 and photolysis (Vione et al., 2009).

Measurements of nitrated phenols have been mainly conducted using offline methods (Harrison et al., 2005a). Air samples are usually collected on filters or cartridges and then analyzed by liquid chromatography (LC) methods (Rubio et al., 2012;Harrison et al., 2005a;Delhomme et al., 2010). These detection methods are time-consuming and measurements as a function of the time of day are not usually possible (Delhomme et al., 2010). The lack of fast-response online measurements has prevented, at least partially, a thorough investigation of sources and sinks of nitrated phenols. Recently, Mohr et al. (2013) deployed a chemical ionization mass spectrometer (CIMS) using acetate as the reagent ion to measure nitrated phenols online in the particle phase in winter in London and based on their measurements the authors concluded that nitrated phenols were mainly from wood burning in this region of the atmosphere.

In this study, we conducted high time resolution measurements of nitrated phenols in the gas phase at a site in an oil and gas production region in winter. High concentrations of ozone and secondary products (Edwards et al., 2014) were observed at

this site, as the result of photochemical degradation of large amounts of alkanes and aromatics emitted from oil and gas production in this region (Warneke et al., 2014). Using the present dataset, we investigate diurnal variations, sources and sinks of nitrated phenols. We use a box model to analyze the budget of nitrated phenols in the atmosphere, and provide insights into the formation mechanism of nitrated phenols.

2. Measurements

The Uintah Basin Winter Ozone Study (UBWOS 2014) was conducted in January and February of 2014 at the Horse Pool site in the Uintah Basin, where over 10,000 active oil and gas wells are located.

2.1 Acetate ToF-CIMS

2.1.1 Instrument operation

An Aerodyne time-of-flight (ToF) CIMS (Lee et al., 2014) that uses acetate ($CH_3C(O)O^-$) as the reagent ion was deployed at the Horse Pool site during the UBWOS 2014 to measure organic acids, inorganic acids and nitrated phenols. These compounds are ionized in the ion-molecule reaction region (IMR, 61.8±0.3 mbar) via proton abstraction (Veres et al., 2008) or by a sequence of clustering-declustering/deprotonation reactions (Brophy and Farmer, 2015) in the reaction with acetate ions. Acetate ions were produced by introducing saturated acetic anhydride/N_2 mixture (5 mL/min) mixed with another flow of N_2 (2.5 L/min) into a polonium-210 (^{210}Po) radioactive source. The instrument was operated at strong de-clustering conditions by applying voltages in the first quadruple ion guide (i.e. SSQ, 2.50±0.01 mbar) during UBWOS 2014, with the ratio of acetate cluster ($CH_3C(O)O^-\bullet CH_3C(O)OH$)/acetate ($CH_3C(O)O^-$) at 0.4%±0.1%. Under such de-clustering conditions, the conjugate anions were usually observed as the product ions, with little contribution from cluster ions. The reagent ions and product ions are analyzed using a high-resolution time of flight mass spectrometer (TOFWERK, Switzerland). The signal of acetate ion was approximately $1\text{-}2\times10^6$ count per second (cps) during the campaign (ToF extraction frequency=25 kHz). The mass resolution for the ToF during UBWOS 2014 was approximately 3200 for ions of m/z >200.

Background signals associated with the instrument were measured every 2 hours for 15 min by passing ambient air through three stages of zero air generation: a platinum catalytic converter heated to 350 °C, nylon wool coated with sodium bicarbonate ($NaHCO_3$), and activated charcoal, which were used in series to remove acidic gases from the sample air and determine instrument backgrounds. During the UBWOS 2014 study, two CIMS inlets constructed from Teflon heated to ~40 °C with similar lengths (~10 m) placed at heights of 1 m and 18.5 m above ground were switched automatically every 30 min during the period of January 24- February 1, to measure the vertical concentration gradient of nitrated phenols and other acidic gases. Inlet switching between a long-heated and a short-unheated inlet was also conducted during February 1-5, to explore possible inlet interferences to CIMS measurements of nitrated phenols from the long-heated inlet. We did not observe differences in signals between the long and short inlets for nitrated phenols except DNP (Figure S1), indicating that potential loss in sampling line was minimal for the reported single nitrated phenols in this study. The inlet issues for DNP will be discussed in Section 2.1.2.

2.1.2 Data processing

The ToF-CIMS data was processed using the TOFware software package (www.tofwerk.com/tofware) written in Igor Pro (Wavemetrics Inc., USA). The detailed data processing procedures are presented in recent studies (Yatavelli et al., 2014;Stark et al., 2015). Post-measurement mass calibrations were performed using nine isolated ions, including m/z 31.9904 (O_2^-), m/z 34.9694 (Cl^-), m/z 44.9982 (CHO_2^-), m/z 59.0139 ($C_2H_3O_2^-$), m/z 61.9884 (NO_3^-), m/z 143.9840 ($C_3F_4O_2^-$), m/z 162.9824 ($C_3F_5O_2^-$), m/z 193.9808 ($C_4F_6O_2^-$) and m/z 243.9776 ($C_5F_8O_2^-$). The four fluorine-containing ions in the list were released from Teflon inlet during UBWOS 2014 and their persistent presence was used for mass calibration. The accuracy of mass calibration was 4.7±1.9 ppm for the whole campaign and the errors of mass calibration for individual ions were usually within 10 ppm (average+3σ). The fitted raw signals for the targeted compounds were normalized using an acetate signal at the level of 1×10^6 cps.

The fitted m/z used for quantification of concentrations of nitrated phenols in the acetate CIMS are m/z 138.0197 ($C_6H_4NO_3^-$) for NP, m/z 152.0353 ($C_7H_6NO_3^-$) for MNP,

m/z 166.0510 ($C_8H_8NO_3^-$) for dimethylnitrophenol+ ethylnitrophenol (DMNP) and m/z 183.0047 ($C_6H_3N_2O_5^-$) for DNP. Compounds with same molecular formulas as nitrated phenols include phenyl nitrates/benzyl nitrates, methoxynitrobenzenes, nitrobenzyl alcohols and hydroxycarboxylic acids derived from pyridine. The first three groups of compounds have lower acidities than acetic acid (Bartmess, 2015) and hence they are unlikely to be observed in acetate CIMS, while hydroxycarboxylic acids derived from pyridine are expected to be small in the atmosphere.

High-resolution (HR) peak fitting to m/z 138, m/z 152 and m/z 183 in the averaged mass spectra of ToF-CIMS on a typical day (January 25, 2014) are shown as examples in Figure 2. Isotope signals from lower masses (dark green lines) accounted for small fractions of the m/z signals. Multiple overlapping ion peaks were identified in the m/z channels. In addition to nitrated phenols, several ions without deprotonation were also present in the even m/z (e.g. $C_8H_{10}O_2^-$ at m/z 138), possibly due to electron transfer reactions and/or fragmentation in the quadrupole ion guides (Stark et al., 2015). The signals of NP and MNP were either the largest or significant larger than their neighboring peaks at their respective m/z, whereas the signal of DNP was much smaller than its neighboring peaks on January 25, 2014. Smaller ratios of the signals between the targeted peak and its neighboring peaks have been shown to deteriorate the precision of fitted signals for the targeted peak (Cubison and Jimenez, 2015;Müller et al., 2011;Corbin et al., 2015). Based on the provided equations in Cubison and Jimenez (2015), the imprecision arising from mass calibration (not including counting error) for the signals of NP, MNP and DNP are 3.2%, 1.8% and 47% based on the mass spectra of January 25, respectively. Imperfect mass calibration can also affect fitted magnitudes of ion signals. Figure S2 shows the sensitivity of the fitted signals of various masses as a function of the errors in mass calibration. The signal changes at a 10 ppm (average+3σ) error of mass calibration relative to perfect mass calibration (error=0 ppm) for NP, MNP and DNP signals are as high as 14%, 5% and 81%, respectively. The results from both precision calculation and sensitivity of fitted magnitudes indicate that the peak signals of NP and MNP can be fitted well with low uncertainties. The peak fitting at m/z 166 for DMNP shows similar results as m/z 138 for NP and m/z 152 for MNP. However, large uncertainties are associated with the peak signals of DNP on January 25, 2014, which is mainly affected

183 by the $C_3F_6HO_2^-$ ions (m/z 182.9886) as indicated by the opposite behaviors of the DNP
184 ion and $C_3F_6HO_2^-$ ion in Figure S2C.

185 The $C_3F_6HO_2^-$ ion (m/z 182.9886) was released from the heated Teflon inlet along
186 with other fluorine-containing ions that were used for mass calibration. The release of
187 $C_3F_6HO_2^-$ ion was supported by much higher signals from the long-heated inlet compared
188 to the short-unheated inlet, when inlet-switching experiments were conducted in February
189 2-5 (Figure S1). Long-heated inlets were used for most of the time during UBWOS 2014
190 (January 23- February 13), except during January 18-22, when a short-unheated inlet was
191 used. The averaged mass spectra of m/z 183 measured on January 18 is shown in Figure
192 2D. Compared to the mass spectra on January 25, $C_3F_6HO_2^-$ signals on January 18 were
193 lower and the signals of DNP were larger than of $C_3F_6HO_2^-$ ions. As a result, the
194 uncertainty from peak fitting for the DNP ion was much lower on January 18 (Figure
195 S2D). Thus, we will only use measured DNP data in the beginning of the campaign
196 (January 18-22), when the long heated inlet was not connected to the acetate CIMS and
197 no inlet switching was performed.

198 The response of the CIMS instrument for nitrated phenols, including 2-NP, 4-NP, 2-
199 methyl-4-nitrophenol and 2,5-dinitrophenol, was calibrated using a Liquid Calibration
200 Unit (LCU, IONICON Analytik). In the LCU, a water solution with known
201 concentrations of the targeted compounds is nebulized and diluted by another gas stream
202 at different flow rates to produce a gas standard at various concentrations (Kaser et al.,
203 2013). The results of the calibrations to various nitrated phenols are shown in Table 1.
204 The sensitivity of 4-NP in our instrument was determined to be higher than that of 2-NP
205 by a factor of 2.1. A higher sensitivity of 4-NP in acetate CIMS was reported in Mohr et
206 al. (2013), but in that study the difference was significantly larger at three orders of
207 magnitude (Mohr et al., 2013). The different sensitivity ratios of 4-NP/2-NP can be
208 caused by many different instrumental conditions between our instrument and that in
209 Mohr et al. (2013), such as the amount of acetic anhydride introduced into instrument,
210 IMR and SSQ pressures, and de-clustering settings in the quadrupole ion guides, all of
211 which affect sensitivities of acetate CIMS significantly (Stark et al., 2012). The main
212 reagent ions in IMR were shown to be acetic acid-acetate clusters rather than acetate
213 (Bertram et al., 2011) and the cluster distributions in IMR may depend on operated

pressure in IMR and the amount of acetic anhydride into the ion source. While de-clustering in SSQ helps the interpretation of recorded mass spectra, de-clustering also obscures a precise understanding of cluster distributions in IMR and hence accurately prediction of sensitivities in acetate CIMS. This result also emphasizes the importance of instrument calibrations in deriving concentration from acetate CIMS. We note that 3-nitrophenol (3-NP) is not usually present in the atmosphere (Harrison et al., 2005a). Thus, the average of the sensitivities of 2-NP and 4-NP was used for calculating concentrations of NP. DMNP was not calibrated in this study and we assumed the same sensitivity as determined for MNP.

The accuracies of nitrated phenols measurements by the CIMS are conservatively estimated to be around 40% for NP and 50% for other nitrated phenols, mainly arising from uncertainties in the concentrations output of the LCU (~10%), uncertainties associated with calibration procedures (~5%), errors in high-resolution (HR) peak fittings to mass spectra (see above and Figure S2), and the representativeness of the calibrated species to other isomers (0-30% for NP and 0-40% for other nitrated phenols). Assuming random errors in the observed ion counts follow a Poisson distribution, detection limits of nitrated phenols, i.e. concentrations with a signal to noise ratio (S/N) of 3, are calculated to be 0.1-0.3 ppt for 1-min average data (Table 1). Following the discussions in Bertram et al. (2011), the measured background ion counts in ToF-CIMS drift over time and thus detection limits are more appropriately calculated as the concentrations at three times of the standard deviation of the measurement background counts. The determined detection limits of nitrated phenols increase to the range of 0.3-0.5 ppt based on this approach (Bertram et al., 2011) (Table 1).

2.2 Other measurements

Volatile organic compounds (VOCs), including hydrocarbons and oxygenates, were measured using an online gas chromatography-mass spectrometer (GC-MS) (Gilman et al., 2013). A commercial proton transfer reaction time of flight mass spectrometer (PTR-TOF) (IONICON Analytik, Austria) was also deployed at the Horse Pool site to measure various VOC species (Warneke et al., 2015). Measurements of phenol, cresols and dimethylphenols+ethylphenols (DMP) were accomplished by the PTR-TOF at m/z

95.0491 ($C_6H_6OH^+$), m/z 109.0648 ($C_7H_8OH^+$) and m/z 123.0804 ($C_8H_{10}OH^+$), respectively. An example of high-resolution peak fitting to m/z 95 in the mass spectra of PTR-TOF is shown in Figure S3. The sensitivities to these phenols are estimated here from the calibrated sensitivities of m/z 93.0699 (toluene), m/z 107.0855 (C8-aromatics) and m/z 121.1012 (C9-aromatics) and the ratio of proton-transfer rate coefficients (k) of the phenols versus the aromatic hydrocarbons (Cappellin et al., 2012) (see details in the SI). Considering the uncertainties in the rate coefficients k, the accuracies of the determined concentrations of phenols can be up to 50% (de Gouw and Warneke, 2007).

Measurements of NO_3 and N_2O_5 were conducted by a cavity ring-down spectroscopy instrument (Dubé et al., 2006). NO_x ($NO+NO_2$), NO_y and O_3 were measured with another cavity ring-down spectroscopy instrument (Wild et al., 2014). Measurements of methane (CH_4) and carbon dioxide (CO_2) were performed with a commercial cavity ring-down spectrometry instrument (Picarro G2301). A pair of commercial spectral radiometers (Metcon Inc.) was used to measure photolysis frequencies of ozone and NO_2.

3. Results and Discussions

3.1 Diurnal variations

Measured diurnal profiles of NP, MNP and DMNP during the UBWOS 2014 are shown in Figure 3. Very strong diurnal variations in concentrations of these nitrated phenols were observed. Concentrations of nitrated phenols were higher at night and lower in the daytime. The ratios between the concentrations in the two hours around midnight (23:00-1:00 MST) and in the two hours around noon (11:00-13:00 MST) are 2.9, 3.9 and 4.7 for NP, MNP and DMNP, respectively. This indicates that the substituted alkyl groups enhance the diurnal variations of nitrated phenols, either through larger source at night or larger sink in the daytime.

Primary emissions of VOCs and NO_x at the Horse Pool site are predominantly due to oil and gas production activities, as the Horse Pool site is surrounded by oil and gas production wells. VOCs and NO_x emitted from nearby oil and gas wells led to periodic concentration spikes during the UBWOS campaigns (Warneke et al., 2014;Yuan et al., 2015). Figure 4 shows two types of episodes encountered during UBWOS 2014. The first

was associated with high concentrations of methane and benzene, as an example of fugitive emissions from oil and gas wells. No enhancement of nitrated phenols was observed for the first emission episode. The second episode was associated with high concentrations of NO_y, NO_x and CO_2, as an example of either vehicle emissions or other fuel combustion activities related to oil and gas extractions (e.g., compressors, dehydrators and pump jacks). High NO_x/NO_y ratios (0.96±0.01) indicate that a fresh combustion plume was encountered. We observed small enhancement of NP during the second emission episode. The enhancement ratio of NP/NO_y in this plume is determined to be $4.6\pm0.7\times10^{-3}$ ppt/ppb, which is comparable with the reported NP/NO_x emission ratios ($1\text{-}50\times10^{-3}$ ppt/ppb) from gasoline and diesel vehicles (Inomata et al., 2013;Sekimoto et al., 2013). Using the obtained enhancement ratio of NP/NO_y, we determine that primary emissions from combustion sources only account for less than 2% of NP concentrations during UBWOS 2014. In addition to these primary sources, biomass burning was not observed in the UBWOS campaigns, based on the absence of any enhancement of biomass burning markers like acetonitrile. We conclude that primary emissions of nitrated phenols were not significant during UBWOS 2014.

In addition to primary emissions, secondary formation from oxidation of phenols is an important source for nitrated phenols (Harrison et al., 2005a). Phenol exhibited a concentration maximum in the afternoon (Figure 3B). The diurnal profile of phenol is more similar to that of secondary acetaldehyde, than that of primary emitted benzene. It suggests that secondary formation was the most important source of phenol. Substituted phenols (cresols and DMP) also had similar diurnal variations as phenol.

3.2 Modeling analysis for NP

3.2.1 Box model results

We will focus on NP to understand the budget of nitrated phenols, because NP had higher concentrations than the substituted nitrated phenols (MNP and DMNP) and there is more information on sources and sinks of NP in the literature. A series of zero-dimensional box model simulations on the formation of phenol and NP were conducted using the online AtChem tool (https://atchem.leeds.ac.uk). The MCM v3.2 (Jenkin et al., 2012) was used as the chemical mechanism in the box model. We note that ambient

304 temperature (-5±5 °C) during UBWOS 2014 was much lower than the temperature
305 (around 25 °C) at which rate constants of many reactions are usually measured. Rate
306 constants as a function of temperature are only available for the reactions of OH radical
307 with benzene and phenol among those shown in Figure 1 and they were already included
308 in MCM v3.2. The model ran in a time-dependent mode and a 48-hour spin-up time was
309 applied in the box model. Measured concentrations of various hydrocarbons, NO_x, O_3,
310 NO_3 and photolysis frequencies (Table S2) were used as constraints in the box model.
311 The simulation period of the model was chosen to be January 18-27, a period associated
312 with several buildup episodes of ozone and other secondary products, with high measured
313 concentrations of NP and without precipitation. Following previous box model studies
314 (Yuan et al., 2015;Edwards et al., 2014), dilution and deposition processes were
315 represented together using a diurnally varying first-order physical loss parameter in the
316 box model. The physical loss rate at night (5.8×10^{-6} s^{-1}) was calculated from the decrease
317 rate of NP concentration between 0:00-6:00 am when the chemical loss was expected to
318 be low (see section 3.3.4). A higher physical loss rate (2.0×10^{-5} s^{-1}) during daytime was
319 used to account for larger turbulent mixing during daytime (Edwards et al., 2014), which
320 results in the decrease of concentrations of inert tracers in the afternoon, e.g. benzene
321 (Figure 3) and methane. Based on sensitivity tests of the box model, increase and
322 decrease of the physical loss rate terms by a factor of two resulted in a -48% and +39% of
323 change in the modeled NP concentrations.

324 As shown in the introduction, photolysis has been recognized as an important sink
325 for nitrated phenols. However, the photolysis of NP (and other nitrated phenols) is not
326 included in the MCM v3.2. We added the photolysis frequency of NP from Bardini
327 (2006) (1.4% of photolysis frequency of NO_2) into the MCM v3.2 and this model run is
328 referred to as the base simulation. Here, we assume that photolysis of NP produces 2-
329 phenoxy biradicals and HONO, as proposed in Bejan et al. (2006) (Figure 1 Route1).
330 There are other possible chemical routes for photolysis of NP: producing phenoxy
331 radicals (C_6H_5O) by losing NO_2 (Route2 in Figure 1) and producing nitrophenoxy radical
332 by hydrogen abstraction (Route3 in Figure 1). The simulation test in Figure S4 indicates
333 that the pathway forming C_6H_5O radicals and NO_2 is an ineffective sink for NP, since
334 C_6H_5O radical will re-form NP by reacting with NO_2. However, we cannot exclude this

pathway to occur along with that producing 2-phenoxy biradicals and HONO. The photolysis frequency determined in Bardini (2006) from concentration changes of 2-nitrophenol in a chamber may not include this pathway as well. As a result, attributing the photolysis rates determined in Bardini (2006) to other pathways other than Route2 is reasonable. The route producing nitrophenoxy radical will be discussed in Section 3.3.

The simulated results for phenol and NP from the base case of the box model are shown in Figure 5. The modeled diurnal variations agreed reasonably well with the observation for both NP and phenol in the base simulation, except for the phenol nighttime levels that will be discussed below. Although modeled NP concentrations are higher than the measurements for both daytime and nighttime, the agreement between measurements and model results is still within their combined uncertainties.

The average measured concentrations of phenol at night are higher than 10 ppt, but the modeled phenol concentrations are usually less than 2 ppt. At night, the production of phenol from benzene oxidation halts, and the fast reaction with NO_3 (2.8×10^{-11} cm^3 $molecule^{-1}$ s^{-1} at 298 K) removes phenol quickly (Figure 7 and discussion in section 3.2.3). Measured nighttime NO_3 radicals were quite low during UBWOS 2014 (1.4±2.4 ppt). As a check on the possible uncertainties in measurements of NO_3 at these low levels, simulations by varying NO_3 concentrations by a factor of 2 result in little improvement for the modeled concentrations of phenol (Figure S5). Another simulation using calculated NO_3 concentrations from the equilibrium between NO_3 and N_2O_5 (Figure S5) also indicates that uncertainties in NO_3 measurements cannot account for the discrepancies between measured and modeled phenol at night. The high phenol concentrations measured at night might be a result of primary emissions. Indeed, the measured phenol concentration was slightly enhanced in the plume with high methane concentrations (see Figure 4A). However, a simulation using the measured phenol concentrations as a constraint in the box model, predicted much higher NP concentrations than measurements (Figure S4). Perhaps a more likely explanation for the enhanced phenol concentrations at night is that the measurements of phenol by PTR-TOF suffer from chemical interferences at night. Vinylfuran might be a candidate (Karl et al., 2007;Stockwell et al., 2015). Thus, the modeled concentrations of phenol shown in Figure 5 will be used in the following discussions.

3.2.2 NO_2 dependence of NP yields

As shown in Figure 1, NP is generated from the reaction of NO_2 with phenoxy radicals ($C_6H_5O\cdot$) (Berndt and Boge, 2003), which is an intermediate from the reactions of OH and NO_3 radicals with phenol and the reaction of phenylperoxy radicals ($C_6H_5O_2$) with NO. In addition to NO_2, $C_6H_5O\cdot$ radicals also react with NO and O_3 (Platz et al., 1998) (see Figure 1), thus the yield of NP has been reported to depend on NO_2 concentrations in the atmosphere (Berndt and Boge, 2003).

In the MCM v3.2, only the reactions of C_6H_5O radical with O_3 and NO_2 are included and here we added the reaction of C_6H_5O with NO (k=1.88×10^{-12} cm^3 molecule^{-1} s^{-1}) for a new simulation. Compared to the base simulation, the modeled concentrations of NP are lower, especially for the period of 11:00-17:00, as the effective yield of NP is reduced (Figure 5). The small enhancement during the period of 11:00-17:00 in NP concentrations from the base simulation is absent in the simulation with the reaction of C_6H_5O with NO. The variations of modeled NP concentrations in the daytime from the new simulation are in better agreement with the measurements (Figure 5). This indicates the reaction of NO and C_6H_5O radical should be considered to account for the NO_2 dependence of NP formation.

Another simulation using fixed NP yields from phenol oxidation reported in Atkinson et al. (1992) (6.7% for OH oxidation and 25.1% for NO_3 oxidation) is also performed. This simulation neglects any dependence of NP yield from phenol oxidation on concentrations of NO_2, O_3 and NO. We observed lower concentrations during both the day and night compared to the base simulation (Figure 5). However, the enhancement of modeled NP in the period of 11:00 -17:00 is distinctly observed with the simulation using the fixed yields in Atkinson et al. (1992), which is in contrast to the lowest concentration in the afternoon from our observations. This, again, indicates there must be a dependence of NP yield from phenol oxidation on NO_2 concentrations in the atmosphere.

3.2.3 Gas-particle partitioning of NP

NP formed in the gas phase can partition into particles (Harrison et al., 2005a). Measurements in several studies demonstrated that 2-NP and MNP were mainly found in the gas phase (Herterich and Herrmann, 1990;Cecinato et al., 2005;Morville et al., 2006).

However, the reported particle fractions of 4-NP and DNP exhibit a broad range in values: the particle fractions of 4-NP and DNP reported in Herterich and Herrmann (1990) were both lower than 15%, whereas most of the concentrations of 4-NP (>75%) (Cecinato et al., 2005) and DNP (>95%) (Morville et al., 2006) were detected in particles in these other two studies.

The concentrations of NP and other nitrated phenols in particles were not measured in this study. We acknowledge that some fractions of nitrated phenols in particles may evaporate into gas phase in the heated inlets. If it holds true, the measured concentrations of nitrated phenols in this study would fall somewhere between concentrations in gas-phase and the total gas+particle concentrations. Here, the gas-particle partitioning of NP as a function of time was estimated using the equilibrium absorption partitioning theory (Pankow, 1994;Donahue et al., 2006) (see details in the SI), based upon pure compound liquid vapor pressure of 2-NP and 4-NP (Schwarzenbach et al., 1988) (Table 2) and measured organic aerosol (OA) concentrations with an aerosol mass spectrometer (AMS). The dependence with temperature was accounted for using the Clausius-Clapeyron relationship with reported enthalpies of evaporation (H_{vap}) (Schwarzenbach et al., 1988). Although vapor pressures from Schwarzenbach et al. (1988) might have significant uncertainties, Schwarzenbach et al. (1988) provided the only comprehensive measurements of sub-cooled liquid vapor pressures of nitrated phenols reported in the literature.

The calculated fractions in particle (F_p) for 2-NP were generally very low (campaign average: $1.1\pm0.9\times10^{-4}$, max: 7.3×10^{-4}), whereas F_p for 4-NP were higher (average: 0.053±0.048, max: 0.38). The variability of the determined F_p values is the result of variations of both OA concentrations (12.5±8.7 μg/m^3, min: <1 μg/m^3, max; 42.6 μg/m^3) and ambient temperature (-5±5 °C, min: -17 °C, max: 10 °C) during the campaign. The higher F_p for 4-NP is expected, as 4-NP (1.4×10^{-3} Torr at 298 K) has much lower vapor pressure than 2-NP (0.20 Torr at 298 K) (Table 2). In addition to absorption, partitioning of NP into aqueous phase of particles is another possible pathway affecting F_p. This mechanism is estimated using Henry's law constants (Sander, 2015) and determined liquid water content (LWC) (8.4±7.5 μg/m^3) in aerosol using the ISORROPIA model (Fountoukis and Nenes, 2007). The estimated F_p values based on aqueous phase

partitioning for 2-NP (1.3×10^{-7}) and 4-NP (3.0×10^{-5}) are both much lower than F_p estimated from the equilibrium absorption partitioning theory, indicating partitioning of NP into particle aqueous phase was not important during UBWOS 2014.

The gas-particle partitioning of 2-NP and 4-NP determined above was incorporated into the box model by constraining the estimated F_p in the determination of gas-particle mass transport rates. The mass transport rates (R_{in} and R_{out}) of a species into and out of particles with radius r are approximated by (Jacob, 2000):

$$R_{in} = \left(\frac{r}{D_g} + \frac{4}{\upsilon\alpha}\right)^{-1} A \times c_g = \frac{1}{\tau} \times c_g \qquad (1)$$

$$R_{out} = \left(\frac{r}{D_g} + \frac{4}{\upsilon\alpha}\right)^{-1} A \times \frac{c_p}{K_{ep}} = \frac{1}{\tau} \times \frac{c_p}{K_{ep}} \qquad (2)$$

where c_g and c_p are concentrations of the species in the gas and particle phase. D_g is the gas-phase molecular diffusion coefficient ($m^2\ s^{-1}$), υ is the mean molecular speed ($m\ s^{-1}$), α is the mass accommodation coefficient. A is the aerosol surface area per unit volume of air ($m^2\ m^{-3}$). K_{ep} is the equilibrium constant, i.e. c_p/c_g, or $/(1-F_p)$. The characteristic time scale of mass transfer (τ) is estimated to be on the order of minutes for particles in the troposphere (Bowman et al., 1997;Jacob, 2000). Thus, rather than determining the characteristic time scale explicitly, we assume that the equilibrium is maintained at each model step (τ=5 min). After entering into particles, no further reaction of NP was prescribed in the model. The modeled diurnal profiles of NP associated with the inclusion of gas-particle partitioning are shown in Figure 6. Compared to the base simulation, the modeled NP concentrations in the gas phase using the estimated F_p from 4-NP are lower (4-8%) for most of the day and slightly higher (2-3%) in the morning when NP concentrations decreased quickly. Since the predicted F_p from 2-NP is very small, the modeled NP concentrations in the gas phase using the estimates from 2-NP were almost identical to the base simulation. In contrast with the modeled concentrations of NP in the gas phase, the modeled total concentrations of NP in gas and particle phase are consistently higher than the base simulation that do not consider gas-particle partitioning. In summary, we observe relatively small changes of the modeled gaseous NP concentrations after the inclusion of gas-particle partitioning in the box model.

Further measurements of the gas/particle partitioning of nitrated phenols are needed to explain the variety of F_p values observed in different studies and/or the potential differences between measurements and prediction from the equilibrium absorption partitioning model.

3.2.4 Budget analysis of phenol and nitrophenol

Diurnal profiles of formation and loss rates derived from the base simulation of the box model for both phenol and NP are shown in Figure 7. Production of phenol only occurs in the daytime from OH oxidation of benzene. The magnitudes of losses of phenol due to OH oxidation (21 ppt/day) and NO_3 oxidation (19 ppt/day) are comparable on a daily basis. From morning to afternoon (8:00-15:00), production of phenol is larger than the losses, resulting in continuous growth of phenol concentrations in this period. After 15:00 pm, the losses start to surpass the production and phenol concentrations decrease quickly. With fast reduction of phenol concentrations in the evening, phenol loss from the reaction with NO_3 is mainly occurred before midnight.

As shown in Figure 7, NP is produced during both daytime and night, with more production in the daytime. As mentioned earlier, the only formation pathway of NP is from the reaction of phenoxy radicals (C_6H_5O) with NO_2, so the contribution from different pathways to NP formation can be derived from source analysis of C_6H_5O radicals (Figure 7C). The production of C_6H_5O radicals is dominated by the reaction of $C_6H_5O_2$ radicals with NO during daytime (71% for 24-hour average) and the reaction of phenol with NO_3 radicals at night (27% for 24-hour average). There are several sources contributing to the formation of $C_6H_5O_2$ radicals in the MCM, including photolysis of benzaldehyde and peroxybenzoic acid, OH oxidation of benzoic acid and phenyl hydroperoxide, and degradations of other radicals (e.g., phenylperoxyacyl radical $C_6H_5CO_3$), suggesting a wide range of aromatic compounds as the precursors of NP in the daytime. The reaction of phenol with OH radicals only accounts for a small fraction of the production of C_6H_5O radicals (2% for 24-hour average), due to the small yield of NP (6%) from the reaction of OH with phenol in the MCM. It indicates phenol is not an important precursor for NP during daytime. The destruction of NP is mainly due to photolysis (17 ppt/day), with some contributions from NO_3 reaction (1.7 ppt/day). The

reaction with OH radicals is not important for the losses of NP in the UBWOS 2014. Dilution/deposition processes account for 20% of the total loss of NP in the box model. Our results are consistent with previous proposal on photolysis as the dominant chemical loss pathway for nitrated phenols (Bejan et al., 2007). Based on the conditions at the Horse Pool site, the lifetime of NP due to photolysis at noontime is calculated to be ~80 min. As the result of the short lifetime of NP during daytime, the production (23.6 ppt/day) and loss rates (23.1 ppt/day) of NP maintain a balanced budget of NP on a daily basis. The inclusion of the reaction of phenoxy radicals (C_6H_5O) with NO discussed in section 3.2.2 would mainly affect NP budget in the noontime, with smaller production and loss in this period.

The different diurnal variations of production and loss rates of NP explain the measured diurnal profile of NP concentrations shown in Figure 3. The increase of loss rates from photolysis result in the quick decline of NP concentrations in the morning. The formation of NP from NO_3 oxidation of phenol in the evening exceeds the destruction of NP, which accounts for the enhancement of NP in this period. The formation and loss rates of NP are comparable in the afternoon and relatively constant concentrations of NP were observed.

A previous study showed that photolysis of nitrated phenols contributes to HONO formation (Bejan et al., 2006). If we assume photolysis of nitrated phenols at rates of 1.4%×J(NO_2) yields HONO at a 100% yield (upper limit), photolysis of NP, MNP and DMNP together accounted for a formation rate of HONO of 1.5±1.9 ppt/hour around noontime (9:00-15:00) during UBWOS 2014. This photolysis source would increase the steady state concentrations of HONO by 0.5 ppt in early morning (7:00-8:30) and 0.2 ppt during the noontime period (9:00-15:00), which are only small fractions of measured HONO concentrations (50-100 ppt) during UBWOS 2014 (Edwards et al., 2014).

3.3 Dinitrophenol

Further oxidation of NP in the presence of NO_x produces DNP. The measured time series of DNP in January 18-22 is shown in Figure 8. A similar diurnal profile was observed for DNP as other nitrated phenols, associated with higher concentrations at night and lower in the daytime. We also notice that the peak time of DNP concentrations

513 at night was somewhat later than NP, consistent with further oxidation of NP as the
514 source of DNP.

515 In the MCM v3.2, reactions of NP with OH or NO_3 radicals generate nitrophenoxy
516 radicals ($NO_2C_6H_5O\cdot$), which react further with NO_2 to form DNP. Here, we assume
517 DNP has the same photolysis rate as NP (1.4% of photolysis frequency of NO_2) (Bardini,
518 2006) and we added the photolysis into the MCM v3.2. The simulated concentrations of
519 DNP from the box model are also displayed in Figure 8. The agreement between
520 measurements and simulation is quite good from the base simulation. DNP has also been
521 observed in the particle phase at significant fractions (Morville et al., 2006). Using the
522 equilibrium absorption partitioning theory described in section 3.3.3 and vapor pressures
523 of two different DNP isomers (2,4-DNP and 2,5-DNP) (Table 2), we incorporated the
524 calculated particle fractions of DNP (Table 2) into the box model as a sensitivity
525 simulation. The predicted DNP concentrations from this simulation are around 5% lower
526 than the base simulation at night. Considering the limited information on DNP formation,
527 the agreement between measured and modeled concentrations of DNP from both
528 simulations is encouraging. This degree of agreement implies that DNP concentrations
529 measured in UBWOS 2014 is explainable by known chemical reactions in the gas phase.

530 As described in Section 3.2, photolysis is the dominant sink for NP and box
531 model results indicate that photolysis of NP may not generate phenoxy radical (by losing
532 NO_2). The other possible product from photolysis of NP is nitrophenoxy radical (Figure 1
533 Route 3), which would act as a secondary source of DNP. This assumption is evaluated
534 as a new simulation. The simulation predicted concentration peaks of DNP in the
535 morning (the orange line in Figure 8), which are not observed in our measurements.
536 Thus, we exclude nitrophenoxy radical as the main products of photolysis of NP.
537 However, the products and exact chemical mechanisms for photolysis of NP remain
538 unclear and thus the photolysis of NP warrants further detailed studies.

539 **3.4 Non-gas phase reactions**

540 The box model only considers gas phase reactions that produce nitrated phenols. In
541 addition to gas phase reactions, aqueous reactions in particles and heterogeneous
542 reactions are other potential sources of nitrated phenols (Harrison et al., 2005a). As

shown in section 3.3.3, using chemical compositions of aerosol at the Horse Pool site and the ISORROPIA model (Fountoukis and Nenes, 2007), the liquid water content (LWC) in aerosol during UBWOS 2014 was estimated to be 8.4±7.5 μg/m^3 (whole campaign average), or 8.4±7.5×10^{-12} expressed as the volume fraction. Based on the box modeling results in Harrison et al. (2005b), aqueous reactions contribute less than 2% of NP production at 3×10^{-9} volume fraction LWC. Thus, aqueous reactions in UBWOS 2014 should not be a significant source for nitrated phenols compared to gas phase reactions.

The Uintah Basin was covered by snow during UBWOS 2014. The importance of heterogeneous reactions on snow surface to formation of nitrated phenols is evaluated using measurements of the vertical gradients of these species. Here, the concentration gradient is defined as the concentrations measured at 18.5 m subtracted from those measured at 1 m. As shown in Figure 9, we observed negative concentration gradients for nitrated phenols at night, indicating that deposition was playing a role and consequently ground snow was a net sink for nitrated phenols at night. A previous study suggested heterogeneous reaction of N_2O_5 with phenol in the aqueous phase produces NP (Heal et al., 2007). Strong deposition of N_2O_5 to the snow surface was observed at night during UBWOS 2014, but as discussed no production of nitrated phenols near the snow surface was detected at night (Figure 9). The vertical gradients for nitrated phenols in the daytime fluctuated around zero with large variations, which might be a result of their low concentrations during daytime. The analysis of vertical gradients implies that heterogeneous reactions on snow surface may not be important for formation of nitrated phenols in the atmosphere during UBWOS 2014.

4. Conclusions

In this study, nitrated phenols in the gas phase were measured using an online acetate ToF-CIMS in an oil and gas production region during winter. Strong diurnal profiles were observed for nitrated phenols, with concentration maxima at night. As the dominant sink for nitrated phenols, photolysis accounted for lower concentrations of nitrated phenols during daytime. We determined that the photolysis of nitrated phenols was not an important source of HONO during UBWOS 2014. Based on box model results, NP was mainly formed in the daytime (73%) from a wide range of precursors,

573 with significant contribution from the reaction of phenol with NO_3 radicals at night
574 (27%). Box model results also indicated that gas phase oxidation of aromatics was able to
575 explain the measured concentrations of NP and DNP. We demonstrated that box model
576 results provided valuable information on the detailed chemical mechanisms in the
577 formation and destruction of NP, e.g., the NO_2 dependence of NP yields from phenol
578 oxidations and chemical products of NP photolysis. We determined that aqueous-phase
579 reactions and heterogeneous reactions were minor sources of nitrated phenols in this
580 study. Although the dataset of nitrated phenols was collected in an oil and gas production
581 region, the chemistry in secondary formation of nitrated phenols and the dynamics of the
582 budget of nitrated phenols in other regions, e.g., urban areas, should behave similarly to
583 those shown in this study.

584 Biomass burning activity did not affect the UBWOS 2014 measurements, and the
585 concentrations of phenols and nitrated phenols were mainly from oxidations of aromatics
586 in the atmosphere. The measurements during UBWOS 2014 provided a great opportunity
587 to study secondary formation of nitrated phenols in the absence of other confounding
588 sources. The UBWOS 2014 campaign also represented the first coincident and high time-
589 resolution measurements of aromatic hydrocarbons, phenols and nitrated phenols in
590 ambient air. The measurements of phenol and nitrated phenols provided a better
591 understanding of their sources, budgets and roles in atmospheric chemistry and for the
592 evaluation of the oxidation mechanisms of aromatics. This is achieved by the emergence
593 of the new ToF-CIMS and PTR-TOF techniques. We envision that these techniques will
594 provide the ability to detect many other intermediate compounds in the atmosphere and
595 that the measurements will advance the understanding of atmospheric oxidation
596 processes.

597

598 ## Acknowledgement

599 The Uintah Basin Winter Ozone Studies were a joint project led and coordinated by the
600 Utah Department of Environmental Quality (UDEQ) and supported by the Uintah Impact
601 Mitigation Special Service District (UIMSSD), the Bureau of Land Management (BLM),
602 the Environmental Protection Agency (EPA) and Utah State University. This work was

603 funded in part by the Western Energy Alliance, and NOAA's Atmospheric Chemistry,
604 Climate and Carbon Cycle program. We thank Questar Energy Products for site
605 preparation and support. Chemical compositions of aerosol were provided by Tim Bates
606 and James Johnson from NOAA Pacific Marine Environmental Laboratory (PMEL) and
607 the Joint Institute for the Study of the Atmosphere and Ocean (JISAO) at University of
608 Washington.
609

References:

Atkinson, R., Aschmann, S. M., and Arey, J.: Reactions of hydroxyl and nitrogen trioxide radicals with phenol, cresols, and 2-nitrophenol at 296 ± 2 K, Environmental Science & Technology, 26, 1397-1403, 10.1021/es00031a018, 1992.

Bardini, P.: Atmospheric Chemistry of Dimethylphenols & Nitrophenols, PhD, University College Cork, Corcaigh, 2006.

Bartmess, J. E.: Negative Ion Energetics Data, NIST Chemistry WebBook, NIST Standard Reference Database Number 69, edited by: Linstrom, P. J., and Mallard, W. G., National Institute of Standards and Technology, Gaithersburg MD, 20899 http://webbook.nist.gov, (retrieved August 28, 2015). 2015.

Bejan, I., Abd El Aal, Y., Barnes, I., Benter, T., Bohn, B., Wiesen, P., and Kleffmann, J.: The photolysis of ortho-nitrophenols: a new gas phase source of HONO, Phys Chem Chem Phys, 8, 2028-2035, 2006.

Bejan, I., Barnes, I., Olariu, R., Zhou, S., Wiesen, P., and Benter, T.: Investigations on the gas-phase photolysis and OH radical kinetics of methyl-2-nitrophenols, Phys Chem Chem Phys, 9, 5686-5692, 10.1039/B709464G, 2007.

Bejan, I., Duncianu, M., Olariu, R., Barnes, I., Seakins, P. W., and Wiesen, P.: Kinetic Study of the Gas-Phase Reactions of Chlorine Atoms with 2-Chlorophenol, 2-Nitrophenol, and Four Methyl-2-nitrophenol Isomers, The Journal of Physical Chemistry A, 119, 4735-4745, 10.1021/acs.jpca.5b02392, 2015.

Berndt, T., and Boge, O.: Gas-phase reaction of OH radicals with phenol, Phys Chem Chem Phys, 5, 342-350, 10.1039/B208187C, 2003.

Bertram, T. H., Kimmel, J. R., Crisp, T. A., Ryder, O. S., Yatavelli, R. L. N., Thornton, J. A., Cubison, M. J., Gonin, M., and Worsnop, D. R.: A field-deployable, chemical ionization time-of-flight mass spectrometer, Atmos. Meas. Tech., 4, 1471-1479, 10.5194/amt-4-1471-2011, 2011.

Bolzacchini, E., Bruschi, M., Hjorth, J., Meinardi, S., Orlandi, M., Rindone, B., and Rosenbohm, E.: Gas-Phase Reaction of Phenol with NO3, Environmental Science & Technology, 35, 1791-1797, 10.1021/es001290m, 2001.

Bowman, F. M., Odum, J. R., Seinfeld, J. H., and Pandis, S. N.: Mathematical model for gas-particle partitioning of secondary organic aerosols, Atmospheric Environment, 31, 3921-3931, http://dx.doi.org/10.1016/S1352-2310(97)00245-8, 1997.

Brophy, P., and Farmer, D. K.: A switchable reagent ion high resolution time-of-flight chemical ionization mass spectrometer for real-time measurement of gas phase oxidized species: characterization from the 2013 southern oxidant and aerosol study, Atmospheric Measurement Techniques, 8, 2945-2959, 10.5194/amt-8-2945-2015, 2015.

Cappellin, L., Karl, T., Probst, M., Ismailova, O., Winkler, P. M., Soukoulis, C., Aprea, E., Mark, T. D., Gasperi, F., and Biasioli, F.: On quantitative determination of volatile organic compound concentrations using proton transfer reaction time-of-flight mass spectrometry, Environ Sci Technol, 46, 2283-2290, 10.1021/es203985t, 2012.

Caralp, F., Foucher, V., Lesclaux, R., J. Wallington, T., and D. Hurley, M.: Atmospheric chemistry of benzaldehyde: UV absorption spectrum and reaction kinetics and mechanisms of the C6H5C(O)O2 radical, Phys Chem Chem Phys, 1, 3509-3517, 10.1039/A903088C, 1999.

Cecinato, A., Di Palo, V., Pomata, D., Tomasi Scianò, M. C., and Possanzini, M.: Measurement of phase-distributed nitrophenols in Rome ambient air, Chemosphere, 59, 679-683, http://dx.doi.org/10.1016/j.chemosphere.2004.10.045, 2005.

Chen, J., Wenger, J. C., and Venables, D. S.: Near-Ultraviolet Absorption Cross Sections of Nitrophenols and Their Potential Influence on Tropospheric Oxidation Capacity, The Journal of Physical Chemistry A, 115, 12235-12242, 10.1021/jp206929r, 2011.

Cheng, S.-B., Zhou, C.-H., Yin, H.-M., Sun, J.-L., and Han, K.-L.: OH produced from o-nitrophenol photolysis: A combined experimental and theoretical investigation, The Journal of Chemical Physics, 130, 234311, doi:http://dx.doi.org/10.1063/1.3152635, 2009.

Corbin, J., Othman, A., D. Allan, J., R. Worsnop, D., D. Haskins, J., Sierau, B., Lohmann, U., and A. Mensah, A.: Peak-fitting and integration imprecision in the Aerodyne aerosol mass spectrometer: effects of mass accuracy on location-constrained fits, Atmospheric Measurement Techniques, 8, 4615-4636, 10.5194/amt-8-4615-2015, 2015.

Cubison, M. J., and Jimenez, J. L.: Statistical precision of the intensities retrieved from constrained fitting of overlapping peaks in high-resolution mass spectra, Atmospheric Measurement Techniques, 8, 2333-2345, 10.5194/amt-8-2333-2015, 2015.

de Gouw, J., and Warneke, C.: Measurements of volatile organic compounds in the earth's atmosphere using proton-transfer-reaction mass spectrometry, Mass Spectrometry Reviews, 26, 223-257, 2007.

Delhomme, O., Morville, S., and Millet, M.: Seasonal and diurnal variations of atmospheric concentrations of phenols and nitrophenols measured in the Strasbourg area, France, Atmospheric Pollution Research, 16-22, 10.5094/APR.2010.003, 2010.

Desyaterik, Y., Sun, Y., Shen, X., Lee, T., Wang, X., Wang, T., and Collett, J. L.: Speciation of "brown" carbon in cloud water impacted by agricultural biomass burning in eastern China, Journal of Geophysical Research: Atmospheres, 118, 7389-7399, 10.1002/jgrd.50561, 2013.

Donahue, N. M., Robinson, A. L., Stanier, C. O., and Pandis, S. N.: Coupled Partitioning, Dilution, and Chemical Aging of Semivolatile Organics, Environmental Science & Technology, 40, 2635-2643, 10.1021/es052297c, 2006.

Dubé, W. P., Brown, S. S., Osthoff, H. D., Nunley, M. R., Ciciora, S. J., Paris, M. W., McLaughlin, R. J., and Ravishankara, A. R.: Aircraft instrument for simultaneous, in situ measurement of NO3 and N2O5 via pulsed cavity ring-down spectroscopy, Review of Scientific Instruments, 77, 034101, doi:http://dx.doi.org/10.1063/1.2176058, 2006.

Edwards, P. M., Brown, S. S., Roberts, J. M., Ahmadov, R., Banta, R. M., deGouw, J. A., Dube, W. P., Field, R. A., Flynn, J. H., Gilman, J. B., Graus, M., Helmig, D., Koss, A., Langford, A. O., Lefer, B. L., Lerner, B. M., Li, R., Li, S. M., McKeen, S. A., Murphy, S. M., Parrish, D. D., Senff, C. J., Soltis, J., Stutz, J., Sweeney, C., Thompson, C. R., Trainer, M. K., Tsai, C., Veres, P. R., Washenfelder, R. A., Warneke, C., Wild, R. J., Young, C. J., Yuan, B., and Zamora, R.: High winter ozone pollution from carbonyl photolysis in an oil and gas basin, Nature, 514, 351-354, 10.1038/nature13767, 2014.

Fernandez, P., Grifoll, M., Solanas, A. M., Bayona, J. M., and Albaiges, J.: Bioassay-directed chemical analysis of genotoxic components in coastal sediments, Environmental Science & Technology, 26, 817-829, 10.1021/es00028a024, 1992.

Fountoukis, C., and Nenes, A.: ISORROPIA II: a computationally efficient thermodynamic equilibrium model for K+ Ca2+ Mg2+ NH4+ Na+ SO42- NO3- Cl- H2O aerosols, Atmos. Chem. Phys., 7, 4639-4659, 10.5194/acp-7-4639-2007, 2007.

Gilman, J. B., Lerner, B. M., Kuster, W. C., and de Gouw, J. A.: Source signature of volatile organic compounds from oil and natural gas operations in northeastern Colorado, Environ Sci Technol, 47, 1297-1305, 10.1021/es304119a, 2013.

Harrison, M. A. J., Barra, S., Borghesi, D., Vione, D., Arsene, C., and Iulian Olariu, R.: Nitrated phenols in the atmosphere: a review, Atmospheric Environment, 39, 231-248, http://dx.doi.org/10.1016/j.atmosenv.2004.09.044, 2005a.

Harrison, M. A. J., Heal, M. R., and Cape, J. N.: Evaluation of the pathways of tropospheric nitrophenol formation from benzene and phenol using a multiphase model, Atmos. Chem. Phys., 5, 1679-1695, 10.5194/acp-5-1679-2005, 2005b.

Heal, M. R., Harrison, M. A. J., and Neil Cape, J.: Aqueous-phase nitration of phenol by N2O5 and ClNO2, Atmospheric Environment, 41, 3515-3520, http://dx.doi.org/10.1016/j.atmosenv.2007.02.003, 2007.

Herterich, R., and Herrmann, R.: Comparing the distribution of nitrated phenols in the atmosphere of two German hill sites, Environ Technol, 11, 961-972, 10.1080/09593339009384948, 1990.

Inomata, S., Tanimoto, H., Fujitani, Y., Sekimoto, K., Sato, K., Fushimi, A., Yamada, H., Hori, S., Kumazawa, Y., Shimono, A., and Hikida, T.: On-line measurements of gaseous nitro-organic compounds in diesel vehicle exhaust by proton-transfer-reaction mass spectrometry, Atmospheric Environment, 73, 195-203, http://dx.doi.org/10.1016/j.atmosenv.2013.03.035, 2013.

Jacob, D. J.: Heterogeneous chemistry and tropospheric ozone, Atmospheric Environment, 34, 2131-2159, http://dx.doi.org/10.1016/S1352-2310(99)00462-8, 2000.

Jenkin, M. E., Saunders, S. M., Wagner, V., and Pilling, M. J.: Protocol for the development of the Master Chemical Mechanism, MCM v3 (Part B): tropospheric degradation of aromatic volatile organic compounds, Atmos. Chem. Phys., 3, 181-193, 10.5194/acp-3-181-2003, 2003.

Jenkin, M. E., Wyche, K. P., Evans, C. J., Carr, T., Monks, P. S., Alfarra, M. R., Barley, M. H., McFiggans, G. B., Young, J. C., and Rickard, A. R.: Development and chamber evaluation of the MCM v3.2 degradation scheme for β-caryophyllene, Atmos. Chem. Phys., 12, 5275-5308, 10.5194/acp-12-5275-2012, 2012.

Karl, T. G., Christian, T. J., Yokelson, R. J., Artaxo, P., Hao, W. M., and Guenther, A.: The Tropical Forest and Fire Emissions Experiment: method evaluation of volatile organic compound emissions measured by PTR-MS, FTIR, and GC from tropical biomass burning, Atmospheric Chemistry and Physics, 7, 5883-5897, 2007.

Kaser, L., Karl, T., Guenther, A., Graus, M., Schnitzhofer, R., Turnipseed, A., Fischer, L., Harley, P., Madronich, M., Gochis, D., Keutsch, F. N., and Hansel, A.: Undisturbed and disturbed above canopy ponderosa pine emissions: PTR-TOF-MS measurements and MEGAN 2.1 model results, Atmos. Chem. Phys. Discuss., 13, 15333-15375, 10.5194/acpd-13-15333-2013, 2013.

Kitanovski, Z., Grgić, I., Yasmeen, F., Claeys, M., and Čusak, A.: Development of a liquid chromatographic method based on ultraviolet–visible and electrospray ionization mass spectrometric detection for the identification of nitrocatechols and related tracers

747 in biomass burning atmospheric organic aerosol, Rapid Communications in Mass
748 Spectrometry, 26, 793-804, 10.1002/rcm.6170, 2012.
749 Lauraguais, A., Coeur-Tourneur, C., Cassez, A., Deboudt, K., Fourmentin, M., and
750 Choël, M.: Atmospheric reactivity of hydroxyl radicals with guaiacol (2-
751 methoxyphenol), a biomass burning emitted compound: Secondary organic aerosol
752 formation and gas-phase oxidation products, Atmospheric Environment, 86, 155-163,
753 http://dx.doi.org/10.1016/j.atmosenv.2013.11.074, 2014.
754 Lee, B. H., Lopez-Hilfiker, F., Mohr, C., Kurtén, T. C., Worsnop, D., and Thornton, J.
755 A.: An Iodide-Adduct High-Resolution Time-of-Flight Chemical-Ionization Mass
756 Spectrometer: Application to Atmospheric Inorganic and Organic Compounds,
757 Environmental Science & Technology, 10.1021/es500362a, 2014.
758 Lin, P., Liu, J., Shilling, J. E., Kathmann, S., Laskin, J., and Laskin, A.: Molecular
759 Characterization of Brown Carbon (BrC) Chromophores in Secondary Organic Aerosol
760 Generated From Photo-Oxidation of Toluene, Phys Chem Chem Phys,
761 10.1039/C5CP02563J, 2015.
762 Mohr, C., Lopez-Hilfiker, F. D., Zotter, P., Prévôt, A. S. H., Xu, L., Ng, N. L., Herndon,
763 S. C., Williams, L. R., Franklin, J. P., Zahniser, M. S., Worsnop, D. R., Knighton, W.
764 B., Aiken, A. C., Gorkowski, K. J., Dubey, M. K., Allan, J. D., and Thornton, J. A.:
765 Contribution of Nitrated Phenols to Wood Burning Brown Carbon Light Absorption in
766 Detling, United Kingdom during Winter Time, Environmental Science & Technology,
767 47, 6316-6324, 10.1021/es400683v, 2013.
768 Morville, S., Scheyer, A., Mirabel, P., and Millet, M.: Spatial and Geographical
769 Variations of Urban, Suburban and Rural Atmospheric Concentrations of Phenols and
770 Nitrophenols (7 pp), Environ Sci Pollut R, 13, 83-89, 10.1065/espr2005.06.264, 2006.
771 Müller, M., George, C., and D'Anna, B.: Enhanced spectral analysis of C-TOF Aerosol
772 Mass Spectrometer data: Iterative residual analysis and cumulative peak fitting,
773 International Journal of Mass Spectrometry, 306, 1-8,
774 http://dx.doi.org/10.1016/j.ijms.2011.04.007, 2011.
775 Natangelo, M., Mangiapan, S., Bagnati, R., Benfenati, E., and Fanelli, R.: Increased
776 concentrations of nitrophenols in leaves from a damaged forestal site, Chemosphere,
777 38, 1495-1503, http://dx.doi.org/10.1016/S0045-6535(98)00370-1, 1999.
778 Olariu, R. I., Klotz, B., Barnes, I., Becker, K. H., and Mocanu, R.: FT–IR study of the
779 ring-retaining products from the reaction of OH radicals with phenol, o-, m-, and p-
780 cresol, Atmospheric Environment, 36, 3685-3697,
781 http://dx.doi.org/10.1016/S1352-2310(02)00202-9, 2002.
782 Pankow, J. F.: An absorption model of the gas/aerosol partitioning involved in the
783 formation of secondary organic aerosol, Atmospheric Environment, 28, 189-193, Doi:
784 10.1016/1352-2310(94)90094-9, 1994.
785 Platz, J., Nielsen, O. J., Wallington, T. J., Ball, J. C., Hurley, M. D., Straccia, A. M.,
786 Schneider, W. F., and Sehested, J.: Atmospheric Chemistry of the Phenoxy Radical,
787 C6H5O(•): UV Spectrum and Kinetics of Its Reaction with NO, NO2, and O2, The
788 Journal of Physical Chemistry A, 102, 7964-7974, 10.1021/jp9822211, 1998.
789 Rippen, G., Zietz, E., Frank, R., Knacker, T., and Klöpffer, W.: Do airborne nitrophenols
790 contribute to forest decline?, Environmental Technology Letters, 8, 475-482,
791 10.1080/09593338709384508, 1987.

792 Rubio, M. A., Lissi, E., Herrera, N., Pérez, V., and Fuentes, N.: Phenol and nitrophenols
793 in the air and dew waters of Santiago de Chile, Chemosphere, 86, 1035-1039,
794 http://dx.doi.org/10.1016/j.chemosphere.2011.11.046, 2012.
795 Sander, R.: Compilation of Henry's law constants (version 4.0) for water as solvent,
796 Atmospheric Chemistry and Physics, 15, 4399-4981, 10.5194/acp-15-4399-2015, 2015.
797 Schwarzenbach, R. P., Stierli, R., Folsom, B. R., and Zeyer, J.: Compound properties
798 relevant for assessing the environmental partitioning of nitrophenols, Environmental
799 Science & Technology, 22, 83-92, 10.1021/es00166a009, 1988.
800 Sekimoto, K., Inomata, S., Tanimoto, H., Fushimi, A., Fujitani, Y., Sato, K., and
801 Yamada, H.: Characterization of nitromethane emission from automotive exhaust,
802 Atmospheric Environment, 81, 523-531, 10.1016/j.atmosenv.2013.09.031, 2013.
803 Stark, H., Yatavelli, R. L. N., Kimmel, J. R., Bertram, T. H., Thornton, J. A., Jimenez, J.
804 L., and Worsnop, D. R.: Cluster Formation and Ion Chemistry in the High Pressure
805 Inlet of a Chemical Ionization Mass Spectrometer: Lessons learned from Field and
806 Laboratory Studies, 22nd International Symposium on Gas Kinetics, June 18-22, 2012,
807 Boulder, CO, 2012.
808 Stark, H., Yatavelli, R. L. N., Thompson, S. L., Kimmel, J. R., Cubison, M. J., Chhabra,
809 P. S., Canagaratna, M. R., Jayne, J. T., Worsnop, D. R., and Jimenez, J. L.: Methods to
810 extract molecular and bulk chemical information from series of complex mass spectra
811 with limited mass resolution, International Journal of Mass Spectrometry,
812 10.1016/j.ijms.2015.08.011, 2015.
813 Stockwell, C. E., Veres, P. R., Williams, J., and Yokelson, R. J.: Characterization of
814 biomass burning emissions from cooking fires, peat, crop residue, and other fuels with
815 high-resolution proton-transfer-reaction time-of-flight mass spectrometry, Atmos.
816 Chem. Phys., 15, 845-865, 10.5194/acp-15-845-2015, 2015.
817 Tremp, J., Mattrel, P., Fingler, S., and Giger, W.: Phenols and nitrophenols as
818 tropospheric pollutants: Emissions from automobile exhausts and phase transfer in the
819 atmosphere, Water Air Soil Pollut, 68, 113-123, 10.1007/BF00479396, 1993.
820 Veres, P., Roberts, J. M., Warneke, C., Welsh-Bon, D., Zahniser, M., Herndon, S., Fall,
821 R., and de Gouw, J.: Development of negative-ion proton-transfer chemical-ionization
822 mass spectrometry (NI-PT-CIMS) for the measurement of gas-phase organic acids in
823 the atmosphere, International Journal of Mass Spectrometry, 274, 48-55, DOI
824 10.1016/j.ijms.2008.04.032, 2008.
825 Vione, D., Maurino, V., Minero, C., and Pelizzetti, E.: Phenol photonitration upon UV
826 irradiation of nitrite in aqueous solution I: Effects of oxygen and 2-propanol,
827 Chemosphere, 45, 893-902, http://dx.doi.org/10.1016/S0045-6535(01)00035-2,
828 2001.
829 Vione, D., Maurino, V., Minero, C., and Pelizzetti, E.: Aqueous Atmospheric Chemistry:
830 Formation of 2,4-Dinitrophenol upon Nitration of 2-Nitrophenol and 4-Nitrophenol in
831 Solution, Environmental Science & Technology, 39, 7921-7931, 10.1021/es050824m,
832 2005.
833 Vione, D., Maurino, V., Minero, C., Duncianu, M., Olariu, R.-I., Arsene, C., Sarakha, M.,
834 and Mailhot, G.: Assessing the transformation kinetics of 2- and 4-nitrophenol in the
835 atmospheric aqueous phase. Implications for the distribution of both nitroisomers in the
836 atmosphere, Atmospheric Environment, 43, 2321-2327,
837 http://dx.doi.org/10.1016/j.atmosenv.2009.01.025, 2009.

838 Warneke, C., Geiger, F., Edwards, P. M., Dube, W., Pétron, G., Kofler, J., Zahn, A.,
839 Brown, S. S., Graus, M., Gilman, J., Lerner, B., Peischl, J., Ryerson, T. B., de Gouw, J.
840 A., and Roberts, J. M.: Volatile organic compound emissions from the oil and natural
841 gas industry in the Uinta Basin, Utah: point sources compared to ambient air
842 composition, Atmos. Chem. Phys., 14, 10977-10988, 10.5194/acpd-14-11895-2014,
843 2014.
844 Warneke, C., Veres, P. R., Murphy, S. M., Soltis, J., Field, R. A., Graus, M. G., Koss, A.,
845 Li, S. M., Li, R., Yuan, B., Roberts, J. M., and de Gouw, J. A.: PTR-QMS vs. PTR-
846 TOF comparison in a region with oil and natural gas extraction industry in the Uintah
847 Basin in 2013, Atmos. Meas. Tech., 8, 411-420, 10.5194/amtd-7-6565-2014, 2015.
848 Wild, R. J., Edwards, P. M., Dube, W. P., Baumann, K., Edgerton, E. S., Quinn, P. K.,
849 Roberts, J. M., Rollins, A. W., Veres, P. R., Warneke, C., Williams, E. J., Yuan, B.,
850 and Brown, S. S.: A Measurement of Total Reactive Nitrogen, NOy, together with
851 NO2, NO, and O3 via Cavity Ring-down Spectroscopy, Environ Sci Technol, 48,
852 9609-9615, 10.1021/es501896w, 2014.
853 Yatavelli, R. L. N., Stark, H., Thompson, S. L., Kimmel, J. R., Cubison, M. J., Day, D.
854 A., Campuzano-Jost, P., Palm, B. B., Hodzic, A., Thornton, J. A., Jayne, J. T.,
855 Worsnop, D. R., and Jimenez, J. L.: Semicontinuous measurements of gas–particle
856 partitioning of organic acids in a ponderosa pine forest using a MOVI-HRToF-CIMS,
857 Atmos. Chem. Phys., 14, 1527-1546, 10.5194/acp-14-1527-2014, 2014.
858 Yuan, B., Veres, P. R., Warneke, C., Roberts, J. M., Gilman, J. B., Koss, A., Edwards, P.
859 M., Graus, M., Kuster, W. C., Li, S. M., Wild, R. J., Brown, S. S., Dubé, W. P., Lerner,
860 B. M., Williams, E. J., Johnson, J. E., Quinn, P. K., Bates, T. S., Lefer, B., Hayes, P. L.,
861 Jimenez, J. L., Weber, R. J., Zamora, R., Ervens, B., Millet, D. B., Rappenglück, B.,
862 and de Gouw, J. A.: Investigation of secondary formation of formic acid: urban
863 environment vs. oil and gas producing region, Atmos. Chem. Phys., 15, 1975-1993,
864 10.5194/acp-15-1975-2015, 2015.
865 Zhang, X., Lin, Y.-H., Surratt, J. D., and Weber, R. J.: Sources, Composition and
866 Absorption Ångström Exponent of Light-absorbing Organic Components in Aerosol
867 Extracts from the Los Angeles Basin, Environmental Science & Technology, 47, 3685-
868 3693, 10.1021/es305047b, 2013.
869
870

Figures

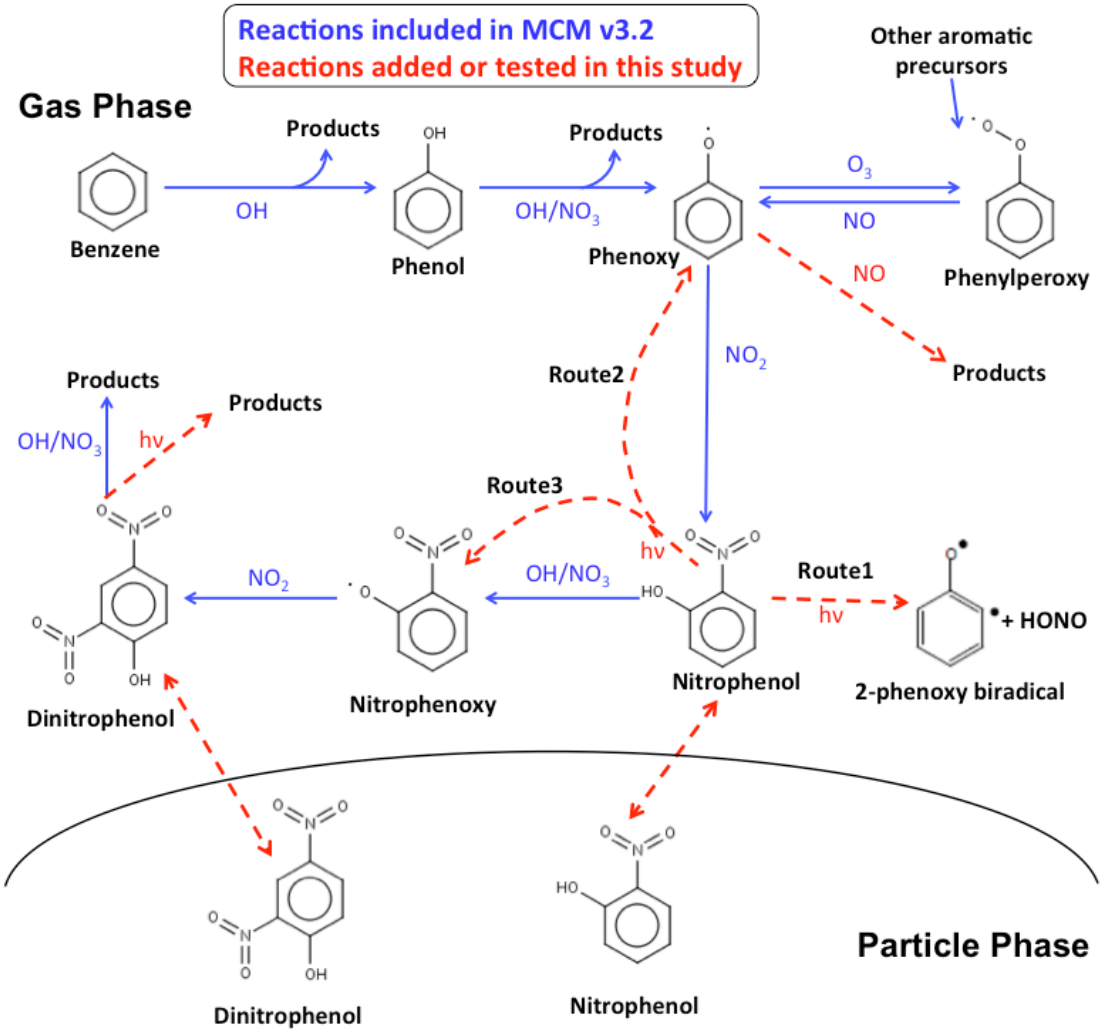

Figure 1. Formation of phenol, nitrophenol (NP) and dinitrophenol (DNP) from the photo-oxidation of benzene in the atmosphere (Jenkin et al., 2003). Reactions in blue are included in the MCM v3.2, whereas reactions in red are added or evaluated in this study. For NP, DNP and the intermediate radicals, other isomers are expected but not shown for the sake of clarity.

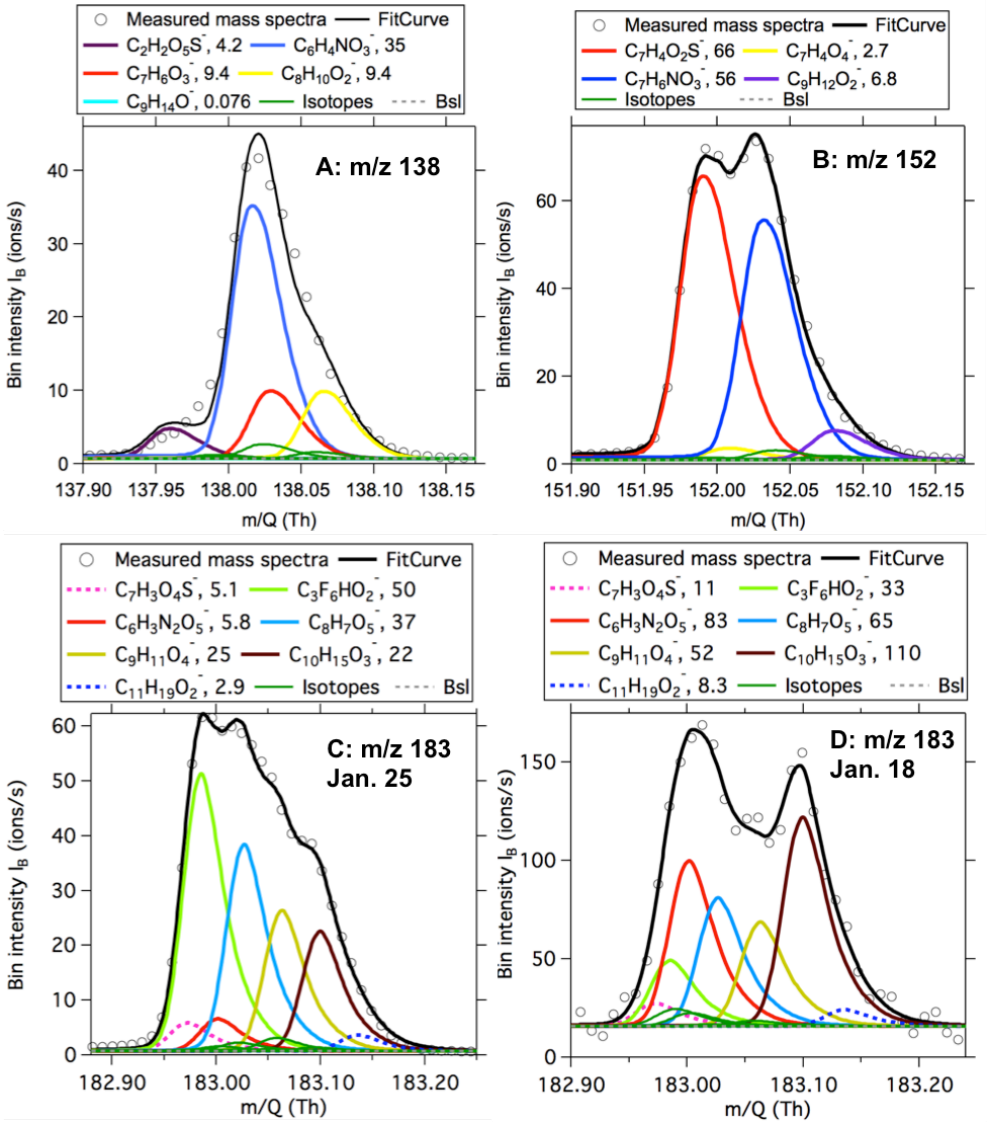

Figure 2. High-resolution peak fitting to the averaged mass spectra of acetate ToF-CIMS for m/z 138 (A), m/z 152 (B) and m/z 183 (C) on January 25, 2014 and m/z 183 (D) on Jan. 18, 2014 during UBWOS 2014. The dark green lines indicate the calculated isotope signals from lower masses.

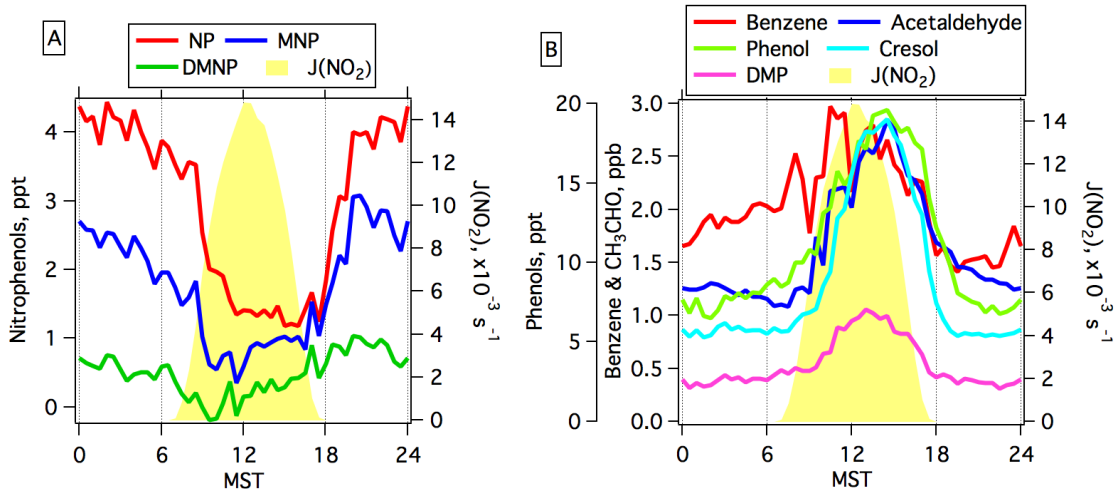

Figure 3. (A) Diurnal profiles of measured NP, MNP, DMNP. (B) Diurnal profiles of benzene, acetaldehyde, phenol, cresol and DMP. Photolysis frequencies of NO_2 are shown in both A and B for reference.

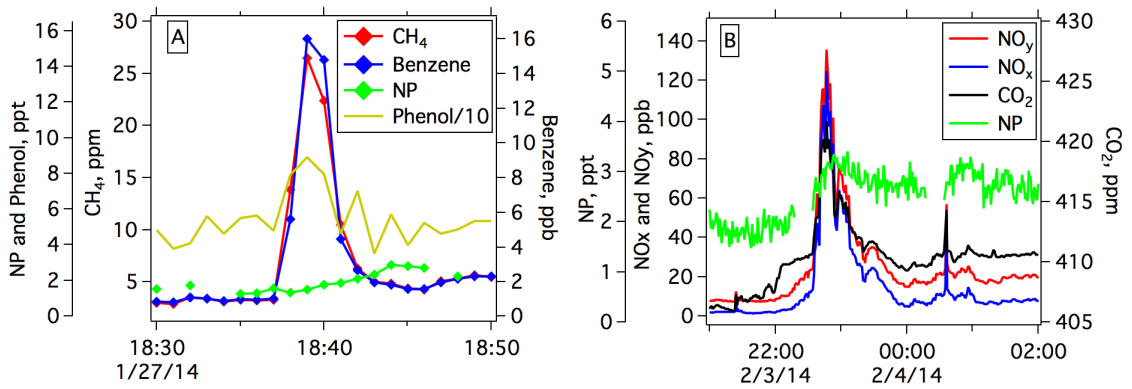

Figure 4. (A) An episode with high concentrations of methane and benzene on January 27, 2014 during UBWOS 2014. The source for this episode was fugitive emissions from oil and gas activities. (B) An episode with high concentrations of NO_y and CO_2 on February 3, 2014 during UBWOS 2014. The source for this episode was fuel combustion (e.g., vehicle exhaust and/or other combustion sources for oil and gas extraction).

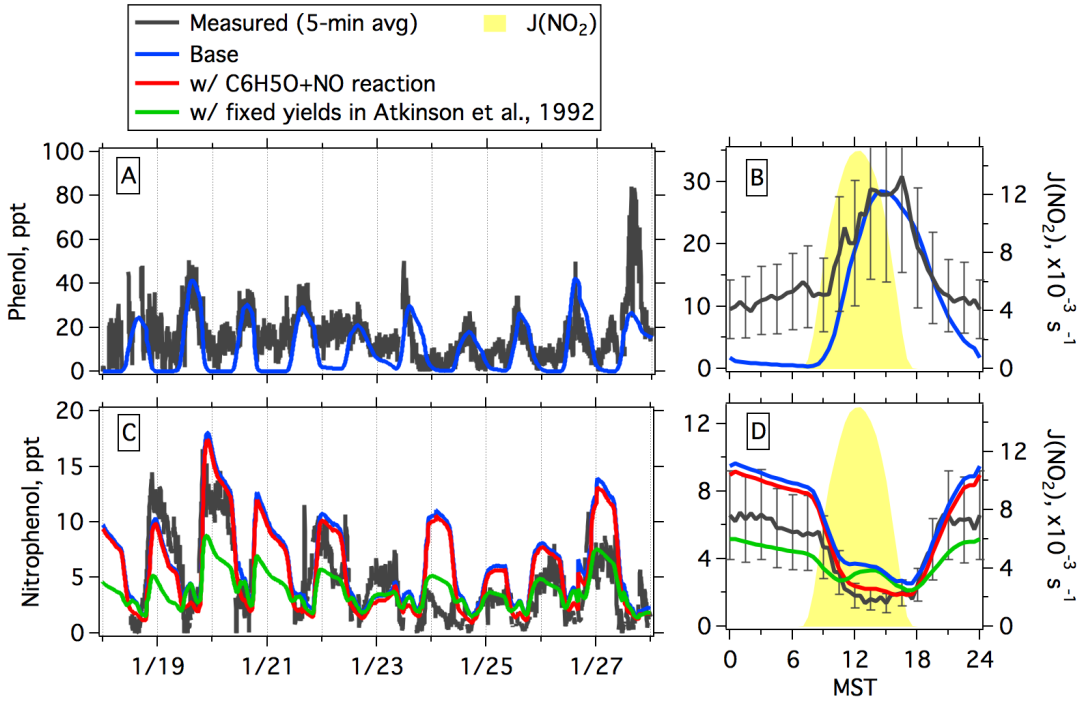

Figure 5. (A and C) Comparison of measured and modeled time series of phenol (A) and NP (C). (B and D) Diurnal profiles of measured and modeled concentrations of phenol (B) and NP (D). Photolysis frequencies of NO_2 are shown in B and D for reference. Error bars in (B) and (D) indicate the accuracies of concentrations of phenol (50%) and NP (40%), respectively.

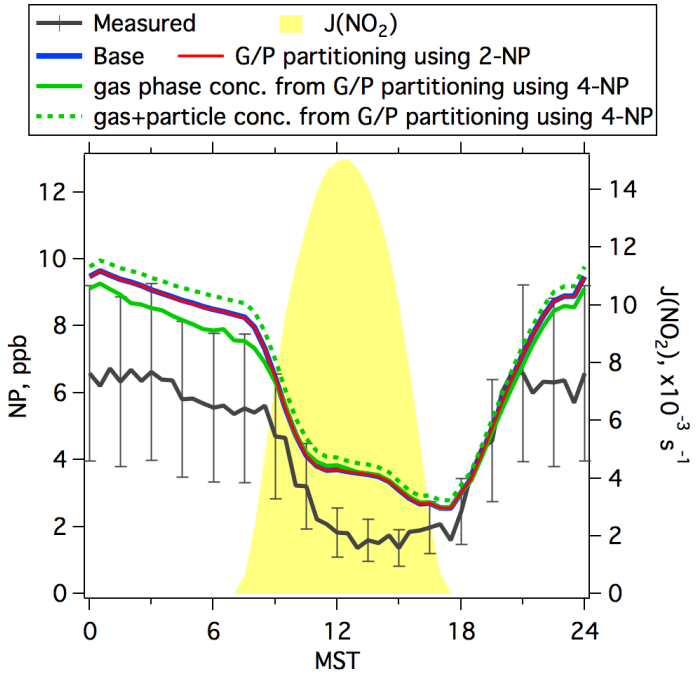

Figure 6. Diurnal profiles of measured and modeled concentrations of NP from the base simulation and the simulations considering gas/particle partitioning. Photolysis frequencies of NO_2 are shown for reference. Error bars indicate the accuracies of concentrations of NP (40%).

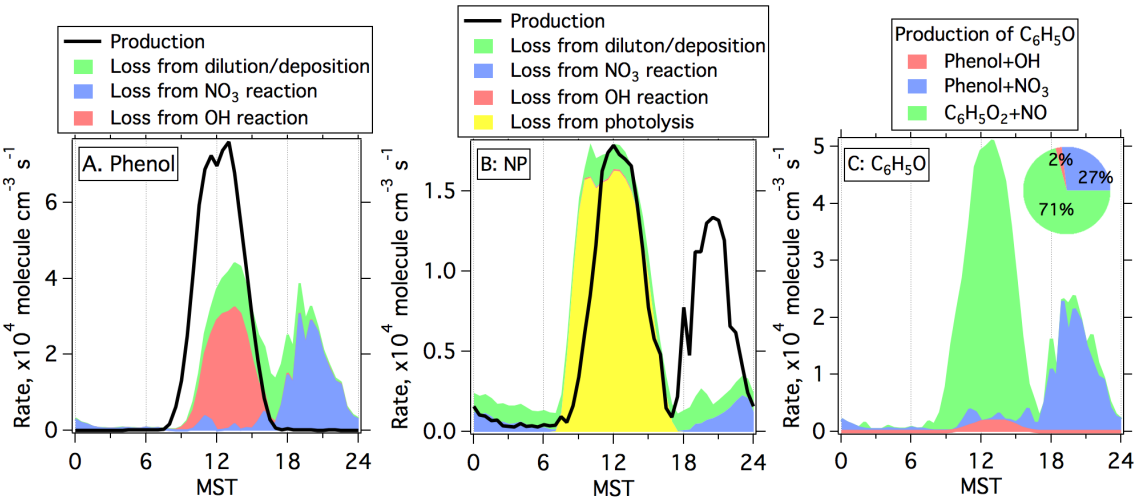

Figure 7. Diurnal profiles of production and loss rates from different pathways for phenol (A) and NP (B) derived from the base simulation of the box model. (C) Diurnal profiles of production rates from different pathways for C_6H_5O radicals. The inserted pie in C shows contributions from three different pathways to the formation of C_6H_5O radicals on a daily basis.

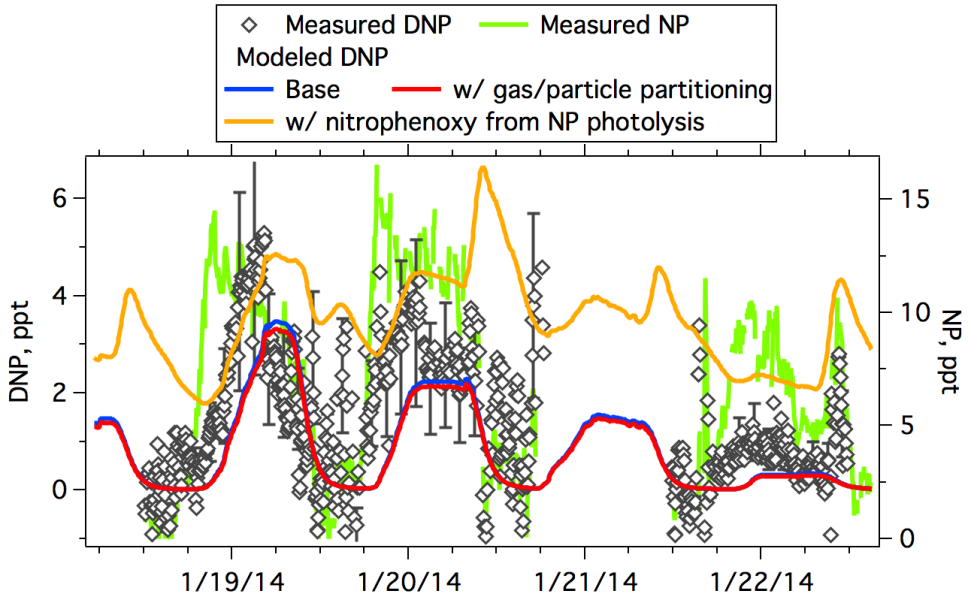

Figure 8. Comparison of measured and modeled time series of DNP. Measured time series of NP is also shown for comparison. Error bars indicate the accuracies of DNP concentrations (50%).

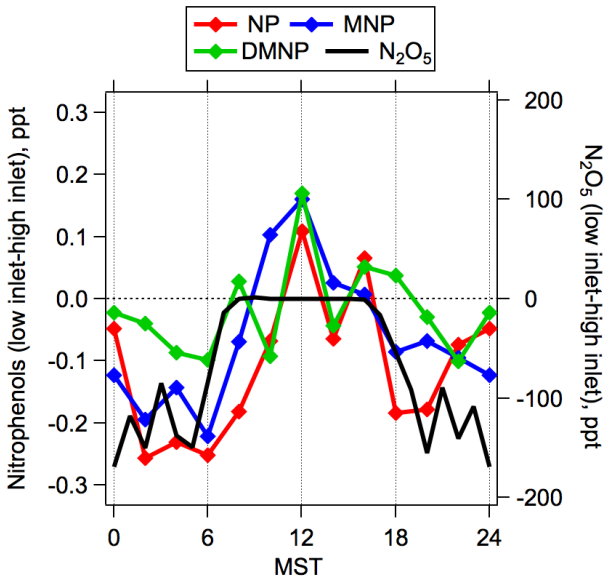

Figure 9. Diurnal profiles of vertical gradients for nitrated phenols measured in January 22 – February 1. The measured vertical gradient of N_2O_5 measured in February 6- 14 is also shown for comparison.

Tables

Table 1. Sensitivities and detection limits of nitrated phenols in acetate ToF-CIMS

Species	Abbreviation	Ion	m/z	Sensitivity, ncps/ppt	Ratio to Formic acid[e]	Detection Limit, ppt[f]	
						Method 1	Method 2
Nitrophenol	NP	$C_6H_4NO_3^-$	138.0197	13.2[a]	2.6	0.18	0.45
Methylnitrophenol	MNP	$C_7H_6NO_3^-$	152.0353	16.6[b]	3.3	0.24	0.36
Dimethylnitrophenol + ethylnitrophenol	DMNP	$C_8H_8NO_3^-$	166.0510	16.6[c]	3.3	0.14	0.36
Dinitrophenol	DNP	$C_6H_3N_2O_5^-$	183.0047	10.3[d]	2.0	0.23	0.58

a: Average from calibrations of 2-NP (8.4 ncps/ppt) and 4-NP (18.0 ncps/ppt).

b: Calibration of 2-methyl-4-nitrophenol.

c: Using the same value as MNP.

d: Calibration using 2,5-dinitrophenol.

e: Based on the determined sensitivity of formic acid at 5.0 ncps/ppt during UBWOS 2014.

f: Method 1 is based on the random errors of observed counts follow Poisson distribution, whereas method 2 is calculated as the concentrations with counts at three times of standard deviations of measured background counts (see discussions in text and in Bertram et al. (2011)).

Table 2. Vapor pressure, enthalpy of evaporation (ΔH_{vap}) and calculated concentration fractions in particle phase (F_p) for several nitrated phenols

Species	Vapor pressure at 298 K, Torr[a]	ΔH_{vap}, kJ/mol[a]	F_p,
2-NP	0.20	53.1	$1.1\pm0.9\times10^{-4}$
4-NP	1.4×10^{-3}	80.0	$5.3\pm4.8\times10^{-2}$
2,4-DNP	8.4×10^{-3}	70.4	$4.6\pm4.4\times10^{-3}$
2,5-DNP	1.2×10^{-3}	68.5	$2.8\pm2.7\times10^{-3}$

a: Calculated from data in Schwarzenbach et al. (1988).